BMC Plant Biology

RESEARCH Open Access

Identification of *HpMYB1* inducing anthocyanin accumulation in *Hippeastrum Hybridum* tepals by RNA-seq

Ji Li[1,2], Kunlin Wu[1], Lin Li[1], Guohua Ma[1], Lin Fang[1,3*] and Songjun Zeng[1,4*]

Abstract

Background Cultivated *Hippeastrum* × *hybridum* is a popular ornamental plant with large and colorful flowers, long flowering duration, and high commercial value. As its main ornamental feature, its flower color is related to the anthocyanin content in the tepals. However, the molecular regulatory mechanisms of anthocyanin biosynthesis in *H.* × *hybridum* have not yet been elucidated.

Results In the present study, 12 cDNA libraries of four stages of *H.*× *hybridum* 'Royal Velvet' tepal development were used for RNA-seq, obtaining 79.83 gigabases (GB) of clean data. The data were assembled into 148,453 unigenes, and 11,262 differentially expressed genes were identified. Forty key enzymes participating in anthocyanin biosynthesis were investigated, and the results showed that most of the anthocyanin structural genes were expressed at low levels in S1 and were markedly upregulated in S2 and S3. The expression profiles of 12 selected genes were verified by qRT-PCR. Furthermore, the R2R3-MYB transcription factor (TF), *HpMYB1*, involved in the regulation of anthocyanin biosynthesis was identified by sequence, expression pattern, and subcellular localization analyses. Its overexpression in tobacco significantly increased the anthocyanin levels in various tissues and activated anthocyanin-related genes.

Conclusions Using RNA-seq technology, we successfully identified a potential R2R3-MYB gene, *HpMYB1*, that regulates anthocyanin biosynthesis in *H.*× *hybridum* 'Royal Velvet'. Our findings provide basic transcript information and valuable transcriptome data for further identification of key genes involved in anthocyanin biosynthesis and can be applied in the artificial breeding of new *H.* × *hybridum* cultivars with enhanced ornamental value.

Keywords Anthocyanins, Transcriptome, *Hippeastrum* × *Hybridum*, Tepal color, R2R3-MYB

*Correspondence:
Lin Fang
linfang@scbg.ac.cn
Songjun Zeng
zengsongjun@scib.ac.cn
[1]Key Laboratory of South China Agricultural Plant Molecular Analysis and Gene Improvement, South China Botanical Garden, Chinese Academy of Sciences, 510650 Guangzhou, China
[2]University of Chinese Academy of Sciences, 100049 Beijing, China
[3]Guangdong Provincial Key Laboratory of Applied Botany, South China Botanical Garden, Chinese Academy of Sciences, 510650 Guangzhou, China
[4]Center of Economic Botany, Core Botanical Gardens, Chinese Academy of Sciences, 510650 Guangzhou, China

Introduction

Flower color is a key characteristic of ornamental crops influenced by the type and content of anthocyanins [1]. Anthocyanins are important secondary metabolites responsible for the purple, blue, and pink colorations of various plant tissues [2]. Nearly 700 anthocyanins have been identified in nature [3], with the six most common being pelargonidin, cyanidin, delphinidin, peonidin, petunidin, and malvidin [4]. Anthocyanins can function as signals to attract pollinators as well as barriers to protect plants from damage, UV rays, and pathogens, and they respond to biotic or abiotic stress [5]. Moreover, anthocyanins act as natural antioxidants and protect against cancer and neuronal or cardiovascular diseases [6, 7]. Because of their numerous benefits, they have been a research hotspot in plant and food sciences.

Anthocyanins are synthesized through the flavonoid pathway, and their structural genes have been extensively studied in many model plants, such as *Arabidopsis thaliana*, *Petunia hybrid*, and *Zea mays* [8–10]. The structural genes encoding multiple enzymes in anthocyanin biosynthesis include chalcone synthase (CHS), chalcone isomerase (CHI), flavonoid-3-hydroxylase (F3H), flavonoid-3'-hydroxylase (F3'H), flavonoid-3', 5'-hydroxylase (F3'5'H), dihydroflavonol 4-reductase (DFR), and anthocyanidin synthase (ANS) [4, 8]. In plant cells, the synthesized hydrosoluble anthocyanins are transported to the vacuoles for long-term stable storage [11].

In plants, the spatial and temporal expression of anthocyanin structural genes is largely regulated by R2R3-MYB, basic helix-loop-helix (bHLH), and WD repeat (WDR) transcription factors (TFs) at the transcriptional level [12, 13], among these, R2R3-MYB TFs are known to be the key regulators of anthocyanin accumulation and tissue coloration and have been identified in model plants. The first R2R3-MYB TF found to regulate anthocyanin biosynthesis was *C1*. It specifically regulates the expression of *CHS* and *DFR* genes in the aleurone layer of maize [14, 15]. Overexpression of *PAP1* upregulates the expression of *CHS*, *CHI*, and *ANS* and significantly increases the content of cyanidin in *Arabidopsis* [16]. *MYB113* and *MYB114* also participate in regulating anthocyanin biosynthesis in *Arabidopsis* [17]. The specific expression of *NtAN2* in *Nicotiana tabacum* not only activates the expression of *CHS* and *DFR* genes, but also co-regulates anthocyanin accumulation with bHLH TF [18]. In addition, similar regulatory systems involved in the accumulation of anthocyanins in ornamental plants have also been identified, including *LhMYB6* and *LhMYB12* in *Lilium* spp. [19], *AaMYB2* in *Anthurium andraeanum* [20], *PeMYB2*, *PeMYB11*, and *PeMYB12* in *Phalaenopsis* spp. [21], *GMYB10* in *Gerbera hybrida* [22], *AcMYB1* in *Aglaonema commutatum* [23], *PsMYB30* and *PsMYB58* in tree peony [24, 25], and *FhPAP1* in *Freesia hybrida* [26].

The genus *Hippeastrum*, commonly known as amaryllis, is a perennial herbaceous bulbous plants belonging to the family Amaryllidaceae [27]. Cultivated *Hippeastrum* × *hybridum* is commercially exploited as an ornamental plant mainly used for Christmas and New Year decorations worldwide because of its large and colorful flowers, long flowering duration, and upright plant architecture [28, 29]. Currently, relevant research on this genus has mainly focused on tissue culture [30], crossbreeding [31], functional components [32], and genetic diversity [33]. *H.* × *hybridum* 'Royal Velvet' is a single-petal flower variety with dark red tepals, which expresses the strongest red petal color and has the highest content of total anthocyanins among the six *H.* × *hybridum* cultivars [34]. Therefore, it is an ideal plant material for studying anthocyanin accumulation and the regulatory mechanism of flower coloration in *Hippeastrum*.

To date, the molecular mechanism of anthocyanin biosynthesis and its effects on tepal coloration in *Hippeastrum* remain unknown because of the lack of reference genome information and high heterozygosity. In the present study, we performed transcriptome sequencing to obtain a global view of the gene expression patterns during the four developmental stages of 'Royal Velvet' tepals. A novel R2R3-MYB gene, *HpMYB1*, was identified by RNA-seq analysis and functionally characterized by overexpression in tobacco. Our results improved our understanding of the potential mechanisms of tepal anthocyanin accumulation and can serve as a basis for further commercial improvement, resource utilization, and molecular breeding of *Hippeastrum* species.

Results

Phenotypes of tepals at different developmental stages

The four stages of 'Royal Velvet' tepal development were analyzed in this study. The tepal color gradually deepened from S1 to S3 and appeared dark red in S3, indicating high accumulation of anthocyanins. In S4, the flowers were in full bloom and remained deep red (Fig. 1A). Moreover, the anthocyanin content and tepal size increased sharply from S1 to S4 and peaked at S4 (Fig. 1B, C).

Sequencing summary, assembly, and unigene annotation

To elucidate the transcriptional mechanism of anthocyanin accumulation in 'Royal Velvet,' the RNA samples obtained from twelve tepal samples were used for transcriptome sequencing with three replicates per development stage. After the low-quality reads were filtered out, a total of 79.83 Gb of clean data and 40,753,960–51,702,956 clean reads were obtained. The Q30 value was >93.11%. (Supplementary Table S1). The Trinity method

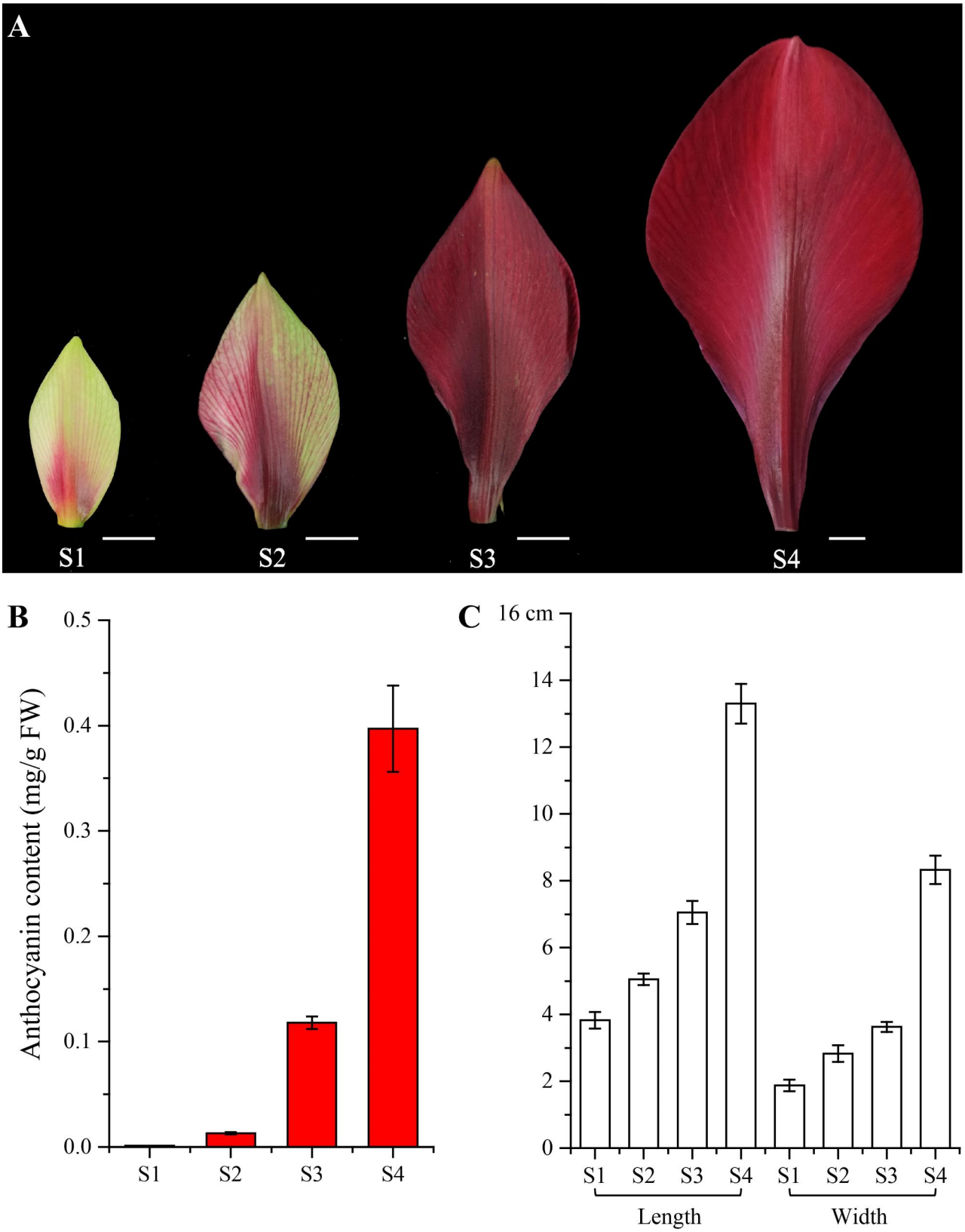

Fig. 1 Phenotypes of tepals at different developmental stages. (**A**) The four stages of *Hippeastrum hybridum* 'Royal Velvet' tepals. Bar = 1 cm. (**B**) The anthocyanin content of tepals at four stages. (**C**) The length and width of tepals at four stages

was used to assemble 148,453 unigenes with a mean length of 739 bp and an N50 of 1116 bp (Supplementary Table S2). Among them, 138,247 (93.13%) unigenes ranged from 200 to 2000 bp in length, and 10,206 unigenes (6.87%) were over 2000 bp in length (Supplementary Table S3). Principal component analysis (PCA) revealed good repeatability between samples, making them suitable for further analysis (Fig. 2A). The unigenes were then subjected to BLAST search against six public databases to determine their potential functions. As a result, 51,769 unigenes (34.87%) were successfully annotated to at least one of the six public databases (Fig. 2B), and the 14 top-hit species based on the NR annotation were listed (Fig. 2C). The KEGG pathway enrichment analysis showed that 'Translation,' 'Carbohydrate metabolism,' and 'Folding, sorting and degradation' were the most significantly enriched categories (Fig. 2D).

Differentially expressed genes (DEGs) analyses

To identify the DEGs involved in 'Royal Velvet' tepal coloration, the TPM values were analyzed at the four developmental stages (FDR≤0.05 and fold change≥2). A total of 11,262 DEGs were identified through pairwise comparisons, of which 5315, 454, and 7170 DEGs were found between S1 vs. S2, S2 vs. S3, and S3 vs. S4, respectively. A Venn diagram analysis of the DEGs indicated that 82 genes were shared among all three comparisons (Fig. 3A). KEGG enrichment analysis was performed to determine the functionality of the identified DEGs. The top 20 enriched KEGG pathways of the unigenes are shown in Fig. 3B–D. Among them, 'Phenylpropanoid biosynthesis,' 'Plant hormone signal transduction,' and 'Flavonoid biosynthesis' were the key pathways involved in pigment accumulation. Besides, DEGs analysis comparing S2, S3, and S4 with S1 and GO enrichment analysis of DEGs were also provided in Supplementary Fig. S2 and S3.

The anthocyanin biosynthesis pathway

Anthocyanin accumulation is one of the most important factors affecting tepal color, especially in red flowers [2]. In the present study, 40 unigenes responsible for anthocyanin biosynthesis were isolated, and expression heatmaps were constructed based on the TPM values (Fig. 4). Thirteen PAL, three C4H, and four 4CL upstream genes involved in anthocyanin biosynthesis were identified, most of which were upregulated in S2 and S3 compared to those in S1 and S4. Seven of the eight *CHS* unigenes were upregulated continuously from S1 to S4, whereas the expression level of all *F3H* unigenes in S4 was lower than that in the other three stages. The predicted unigenes included two *F3'H*, two *DFR*, one *ANS*, and one *UFGT* were screened as late biosynthesis genes (LBGs),

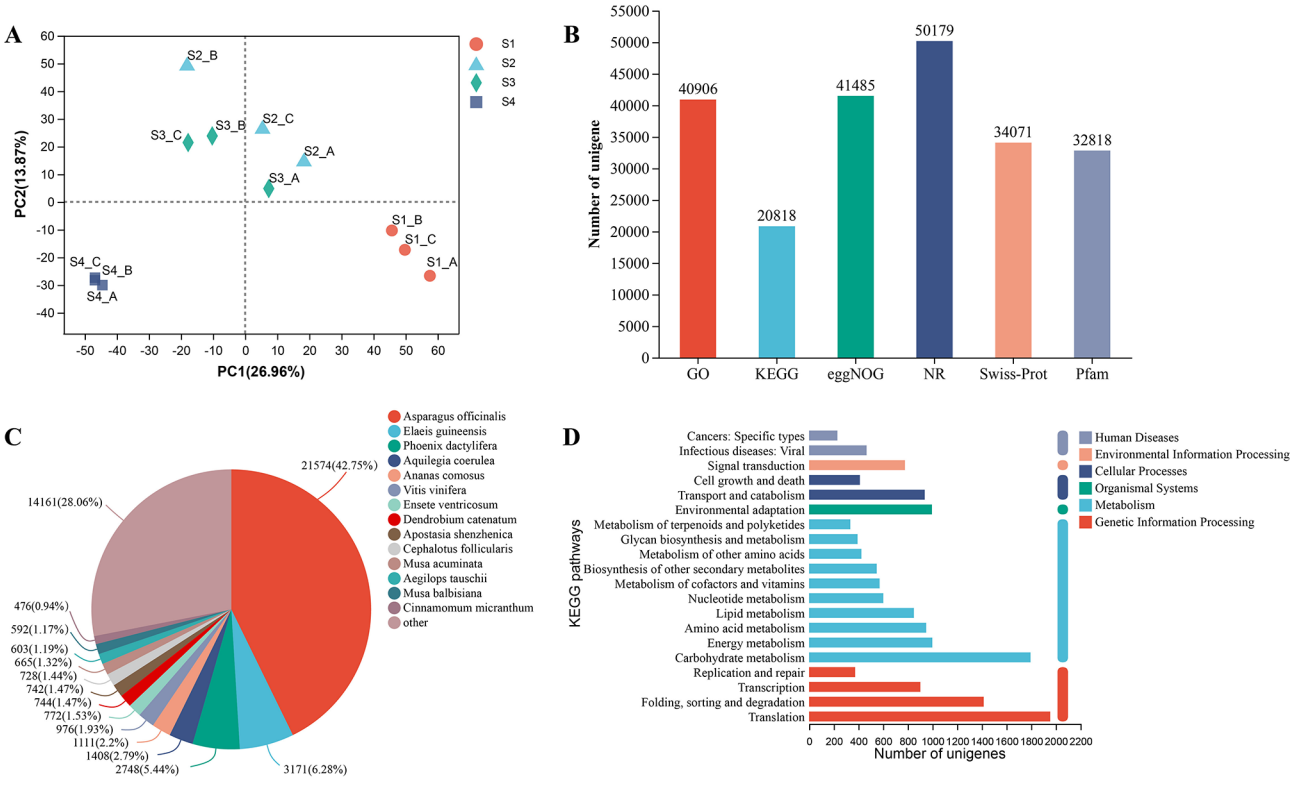

Fig. 2 Overview of RNA-seq results and unigene annotations. (**A**) Principal components analysis of unigene expression in *Hippeastrum hybridum* 'Royal Velvet' tepals. (**B**) Functionl annotation of unigenes in six public database. (**C**) Species distribution of unigenes in the NR database. (**D**) The unigenes functional classifcation in KEGG databases

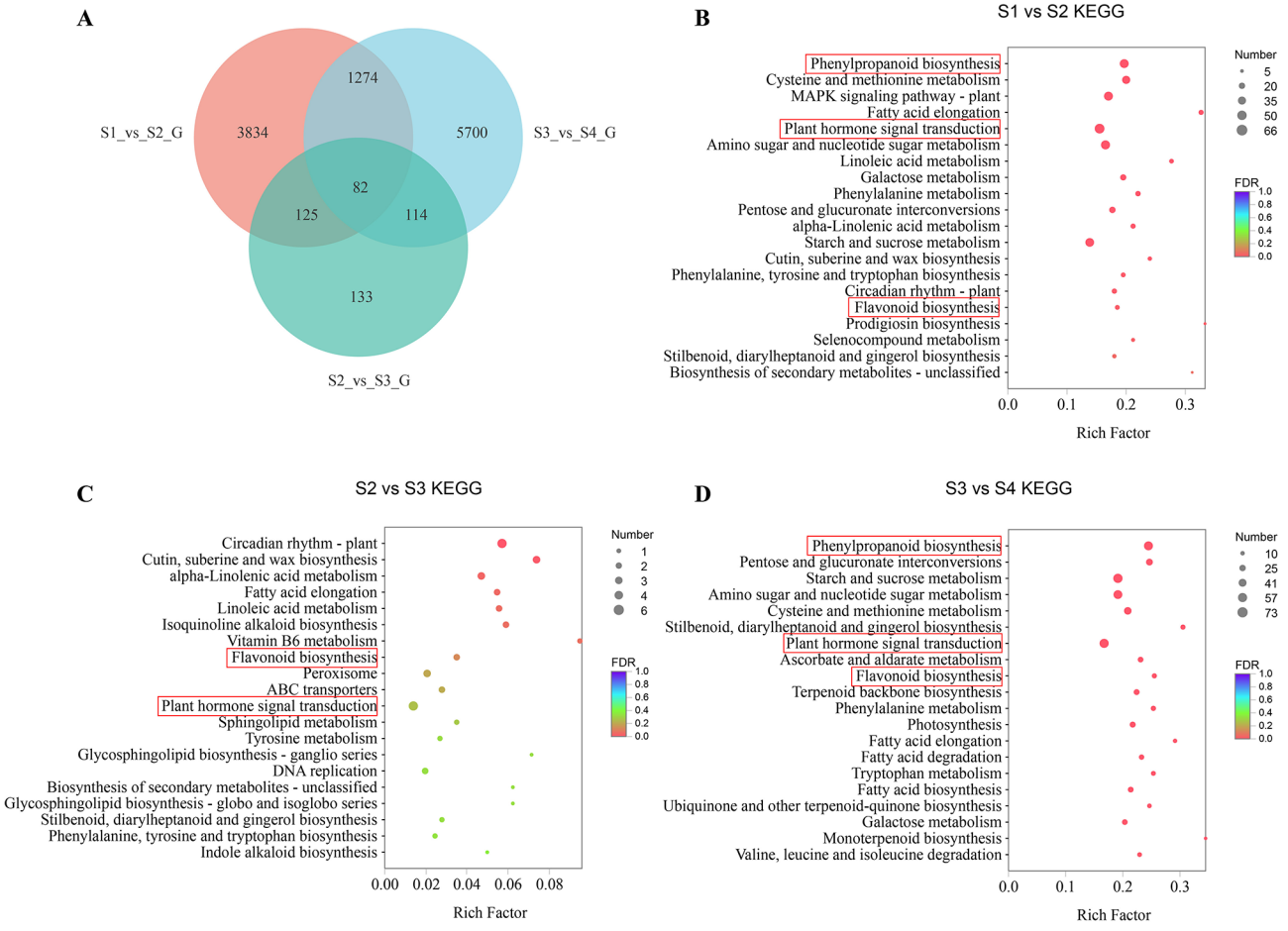

Fig. 3 Venn diagram and functional analysis of DEGs in *Hippeastrum hybridum* 'Royal Velvet'. (**A**) Venn diagram analysis of DEGs per comparison. (**B**-**D**) KEGG enrichment of DEGs per comparison. The red boxes indicate key pathways that may participated in pigment accumulation

and most of them (except for TRINITY_ DN10291_c0_g1 and TRINITY_DN3411_c1_g1) were down-regulated in S1 compared with those in S2 to S4. The detailed TPM values for each unigene are provided in Supplementary Table S4.

To validate the credibility of the transcriptome sequencing data, 12 unigenes were selected from the anthocyanin biosynthesis pathway, and their expression levels were analyzed at four stages using qRT-PCR (Fig. 5). Our qRT-PCR results were consistent with those obtained using the RNA-seq method, indicating that the use of RNA-seq for counting reads was reliable for further analysis.

Identification of key TFs in regulating anthocyanin biosynthesis in the tepals of *H.* × *hybridum* 'Royal Velvet'

Transcription factors (TFs) play a major role in color formation by regulating the expression of key enzymes involved in anthocyanin biosynthesis. In our study, 1187 TFs belonging to 33 families were identified and classified using RNA-seq annotation. MYB (198), AP2/ERF (126), and C2C2 (88) were the top three TF families by number (Fig. 6A).

Furthermore, MYB TFs were studied to deepen our understanding of their involvement in the regulation of dark red color formation at the four developmental stages of 'Royal Velvet' tepals. Heatmaps of the 198 MYB TFs were constructed and the TFs were divided into ten clusters based on their expression profiles (Fig. 6B and C). The results showed that the expression patterns of MYB TFs in cluster 2 were significantly positively correlated with the changes in most anthocyanin structural genes at the four developmental stages. Furthermore, the expression patterns and sequence homology of the 11 unigenes from cluster 2 were analyzed, and one unigene with ID TRINITY_DN4295_c0_g1 had an R2R3 DNA-binding domain and high homology with known positive anthocyanin regulators in other plants. Thus, this unigene was selected as a potential MYB TF involved in the regulation of anthocyanin biosynthesis to be investigated in the subsequent study.

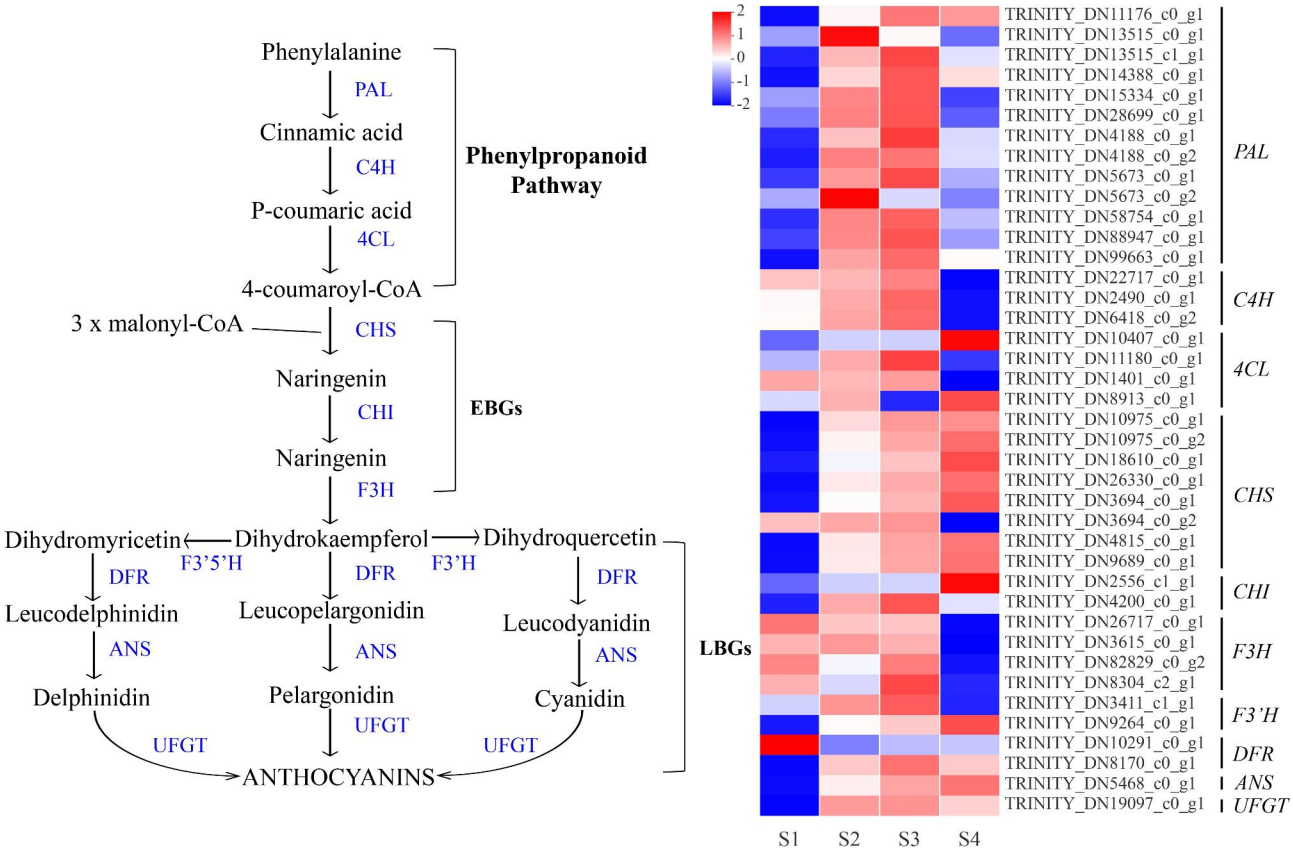

Fig. 4 Heatmap constructed using anthocyanin biosynthesis related unigenes. The heatmap is generated based on the mean expression levels of anthocyanin structural gene using the TPM values from RNA-seq. Blue represents low expression levels, while red signifies high expression levels. EBGs: early biosynthesis genes; LBGs: late biosynthesis genes; PAL: phenylalanine ammonia-lyase; C4H: trans-cinnamate 4-monooxygenase; 4CL: 4-coumarate-CoA ligase 2; CHS: chalcone synthase; CHI: Chalcone isomerase; F3H: Flavanone 3-hydroxylase; F3'H: favanone 3-hydroxylase; F3'5'H: flavonoid 3', 5'- hydroxylase; DFR: dihydrofavonol 4-reductase; ANS: anthocyanidin synthase; UFGT: UDP-favonoid glucosyl transferase

Isolation and sequence analysis of *HpMYB1*

Based on the RNA-seq data, the sequences of the unigene TRINITY_DN4295_c0_g1 from the tepals of 'Royal Velvet' were cloned by PCR and designated as *HpMYB1* (GenBank accession number: OQ446482). *HpMYB1* has a 696-bp open reading frame (ORF) and encodes 231 amino acids. A bootstrapped phylogenetic tree generated using MEGA 7.0 with the neighbor-joining method showed that HpMYB1 clustered with AcMYB1, FhPAP1, and MybA in the AN2 subgroup (Fig. 7A). Multiple amino acid sequence alignment of HpMYB1 and other known positive anthocyanin regulators showed that the conserved R2 and R3 domains were located at the N-terminus, and a conserved bHLH motif interacting with a bHLH TF was located in the R3 domain (Fig. 7B). The GenBank accession numbers from this study are provided in Supplementary Table S6.

Expression patterns and subcellular localization of *HpMYB1*

The transcript levels of *HpMYB1* and anthocyanin concentration in the four stages of tepal development and in different tissues of 'Royal Velvet' were monitored. The results showed that *HpMYB1* mRNA was highly expressed in the tepals at all four developmental stages, in which anthocyanins were highly accumulated, whereas no or trace amounts of *HpMYB1* mRNA were detected in the tissues with no anthocyanin accumulation, such as roots, bulb scales, leaves, or pedicels (Fig. 7C). These results strongly suggested that *HpMYB1* expression was correlated to the anthocyanin accumulation in 'Royal Velvet.'

To function as a regulator, HpMYB1 must be located inside the nucleus of plant cells. Thus, subcellular localization analysis of the HpMYB1 protein was performed. HpMYB1 was fused to a yellow fluorescent protein (YFP) and cloned into the pSAT6-EYFP-N1 vector. The YFP fluorescent signal of recombinant 35 S::HpMYB1-YFP was detected in the nucleus, similar to the nuclear localization marker mCherry (Fig. 7D). These results confirmed that HpMYB1 is localized in the nucleus.

Effects of HpMYB1 overexpression in Tobacco

To characterize the role of HpMYB1 in the regulation of anthocyanin biosynthesis, *HpMYB1* driven by the

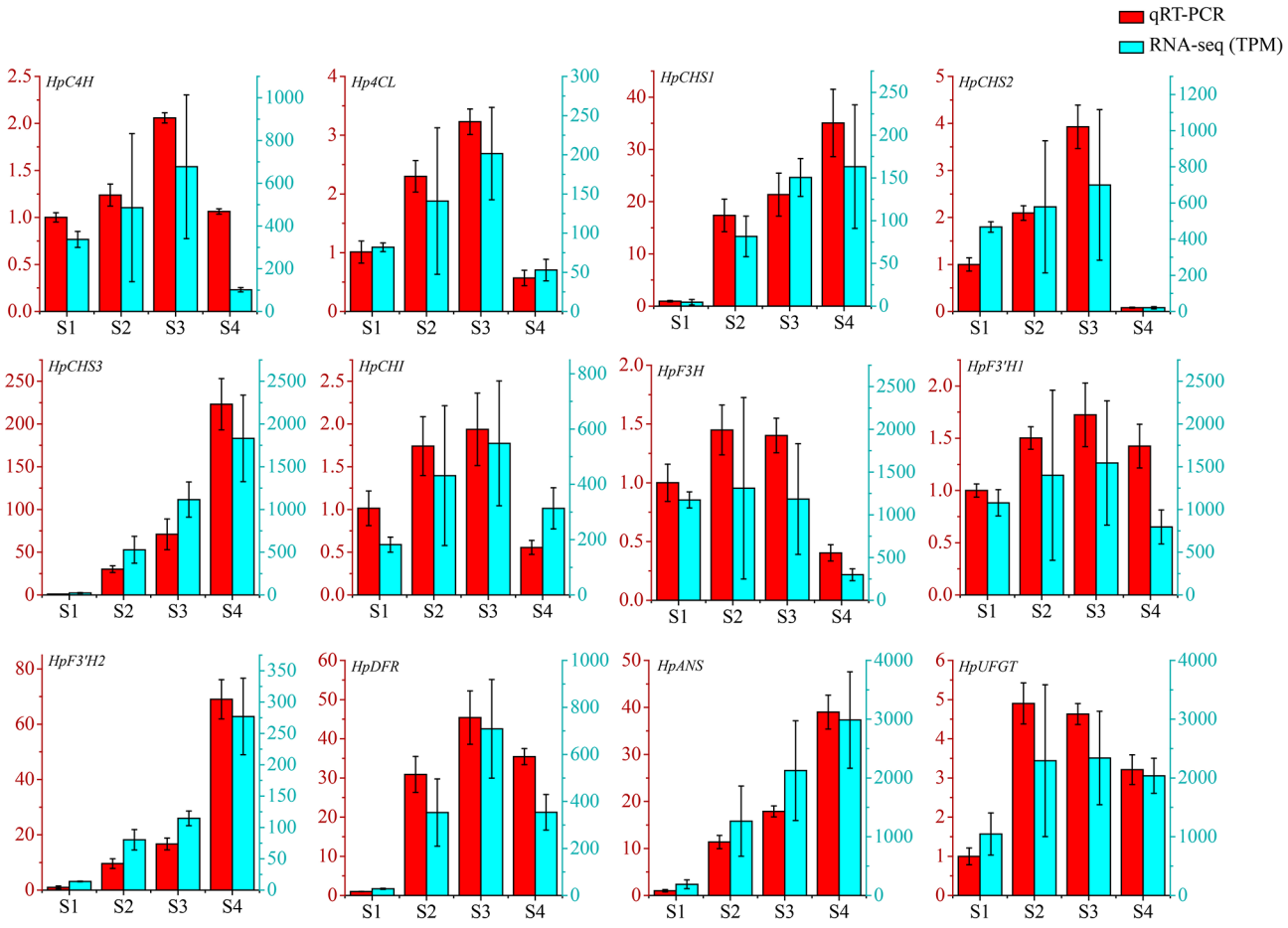

Fig. 5 qRT-PCR verifcation of the expression profles of selected unigenes involved in anthocyanin biosynthesis. Twelve unigenes from the anthocyanin biosynthesis pathway were used to validate the RNA-seq results. The expression levels were calculated by the $2^{-\Delta\Delta CT}$ method. The y-axis on the left represents the unigene relative expression by qRT-PCR and the y-axis on the right indicates the TPM value of the unigene in RNA-seq data. The unigene ID and specific primers were provided in Supplementary Table S5

constitutive CaMV 35 S promoter was introduced into tobacco leaf discs via *Agrobacterium*-mediated transformation, and significant phenotypic changes in both vegetative and reproductive tissues were observed in the transgenic lines. In comparison with the reproductive tissues of the wild type, darker corollas, pigmented filaments, anthers, pistils, calyces, ovaries, and seed coats were observed in the HpMYB1 overexpression lines (Fig. 8A, C, and E). Similarly, the leaves and roots conferred an intense red-purple color upon *HpMYB1* overexpression tobacco (Fig. 8B, D). The total anthocyanin content in the leaves and corollas of the *HpMYB1* transgenic lines was higher than that of the control (Fig. 8G and I).

To confirm the target genes of HpMYB1, a qRT-PCR analysis was performed on the leaves and corollas of both transgenic tobacco and control plants to analyze the expression levels of genes involved in the anthocyanin pathway, including nine structural genes and two bHLH TF regulators. The results indicated that all 11 genes related to anthocyanin biosynthesis were markedly upregulated in the leaves of all three transgenic lines compared to those in the control (Fig. 8F). Likewise, the transcript abundances of these 11 anthocyanin-specific genes were significantly higher in the corollas of the three transgenic lines than in those of the control (Fig. 8H). These results suggested that HpMYB1 is a functional MYB TF factor that regulates anthocyanin biosynthesis.

Discussion

Application of transcriptome sequencing for studying the anthocyanin regulation mechanism of *H.* × *hybridum* 'Royal Velvet' tepals

H. × *hybridum*, a species of the genus *Hippeastrum*, has high ornamental value and is popular worldwide [28, 29]. For nearly 200 years, breeders have committed themselves to cultivating new *Hippeastrum* hybrid species [31]. However, the lack of reference genome data and high heterozygosity have greatly limited the research on the molecular mechanisms of key trait formation in this

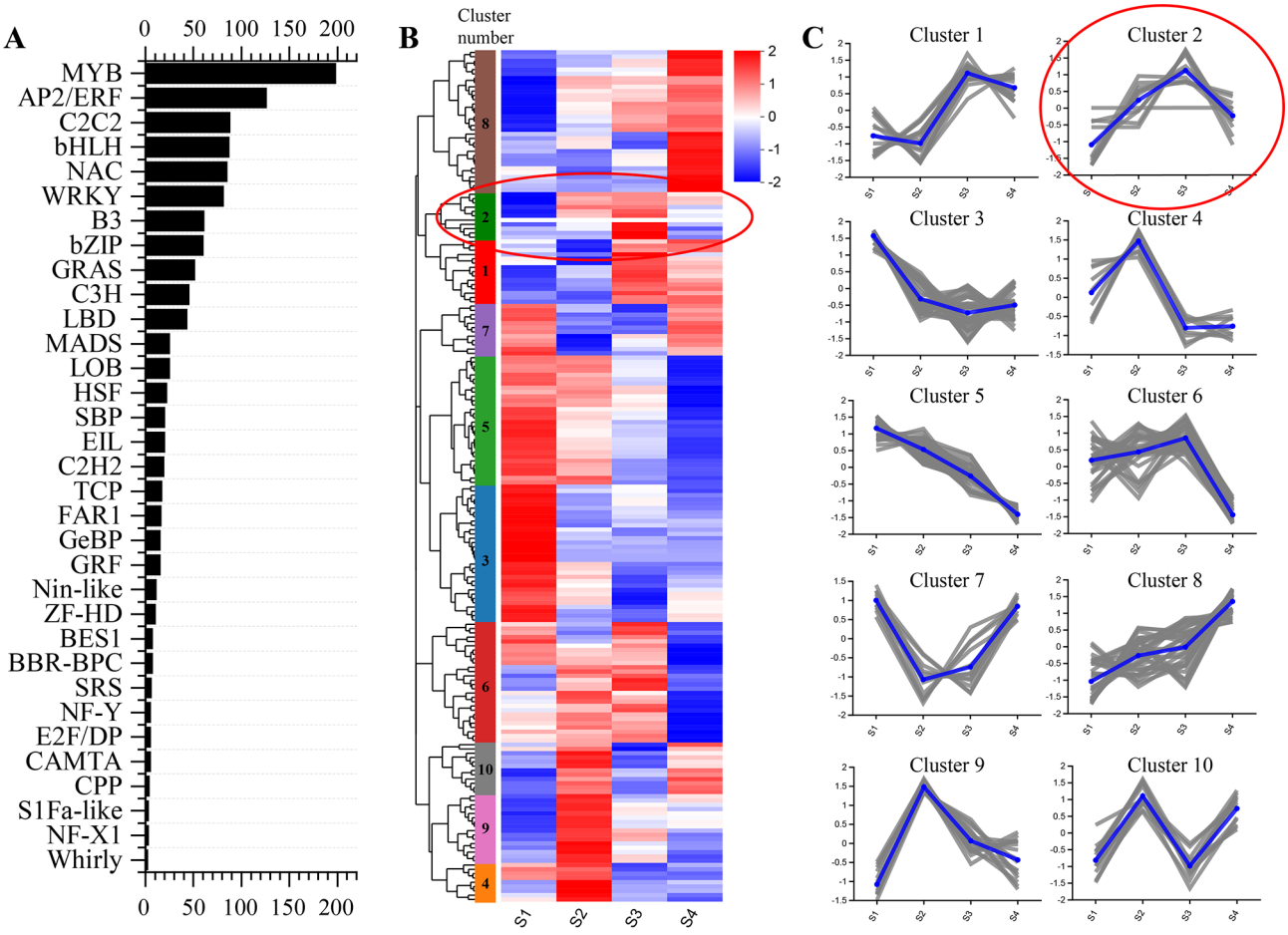

Fig. 6 Analysis of transcription factors based on transcriptome sequencing. (**A**) Top 20 transcription factor families in *Hippeastrum hybridum* 'Royal Velvet' tepals. (**B**) Heatmaps showing the expression profile of 198 MYB, based on standardized TPM values. Ten different color modules represent different clusters and cluster 2 was circled in a red oval. (**C**) 198 MYB were grouped into ten clusters depending on the expression profile. the y-axis represent the normalized expression

genus. Transcriptome sequencing provides a low-cost, rapid, and reliable method to monitor gene expression patterns and identify key genes at various developmental stages or under different physiological conditions in non-model plants lacking genomic information [35, 36]. In grape hyacinth, transcriptome sequencing of the blue and white variants provided a foundation for future functional and molecular biological studies on flower color [37]. In *Dendrobium nestor*, a transcriptomic analysis of petal samples from three developmental stages helped discover the key candidate genes of the anthocyanin pathway and revealed the mechanism of purple color formation [38]. In the present study, we applied the transcriptome sequencing technology to perform a global transcript analysis of the four tepal development stages of *H.* × *hybridum* 'Royal Velvet' and investigate the molecular mechanism underlying the anthocyanin regulation and dark red flower color formation in this species. Finally, we annotated 148,453 unigenes with an annotation rate of 34.87% to at least one of the six public databases, which was similar to those of other *H.* × *hybridum* [33, 39] and *Amaryllidaceae* species [40, 41]. Our transcriptome sequencing also provided global gene expression data for further studies on *H.* × *hybridum* 'Royal Velvet.'

Floral color and key structural genes in the anthocyanin biosynthesis of *H.* × *hybridum* 'Royal Velvet'

In *H.* × *hybridum*, flowers provide visual attractiveness, and the commercial value of ornamental plants is largely related to their tepals. Anthocyanins are the major pigments that confer red, blue, and purple coloration to various plant tissues [42, 43]. Accumulation of anthocyanins can be closely associated with flower color. In *Hydrangea macrophylla*, the infertile blue flower color is mainly correlated with an increase in anthocyanin content [44]. In buckwheat, higher anthocyanin accumulation was detected in the cotyledons and flowers of the red cultivar than in those of the white cultivar at different growth stages [45]. A similar phenomenon has been reported

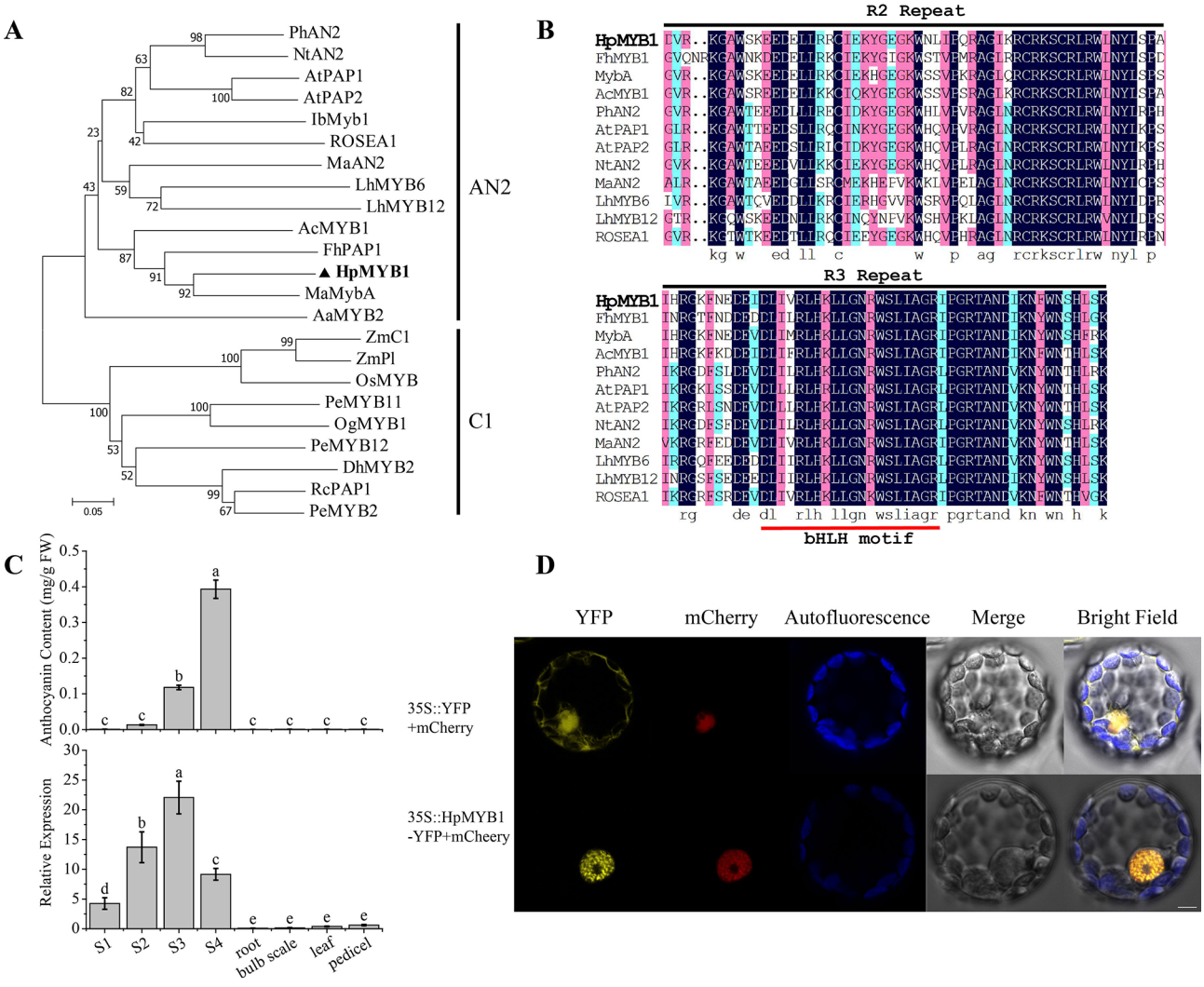

Fig. 7 Sequence, expression patterns and subcellular localization analysis of HpMYB1. (**A**) Phylogenetic tree of HpMYB1 and 22 other known anthocyanin-related R2R3-MYBs in other plants. (**B**) Multiple alignment of the conserved R2-domain and R3-domain of different anthocyanin biosynthesis related R2R3-MYB proteins. The black line showed the conserved R2 and R3 domain, The red line indicated a motif ([D/E]Lx$_2$[R/K]x$_3$Lx$_6$Lx$_3$R) interacting with a bHLH TF. (**C**) The anthocyanin content and the relative expression of *HpMYB1* at different tepal developmental stages and different tissues. (**D**) Subcellular localization of HpMYB1 protein in *Arabidopsis thaliana* mesophyll protoplasts. Bar = 5 μm, YFP: yellow fluorescence protein; mCherry: nuclear localization

in azalea [46], *Camellia sinensis* [47], and pagoda trees [48]. In the present study, the anthocyanin content in the tepals of 'Royal Velvet' at four flowering stages was determined for the first time. With the rapid increase in total anthocyanin levels from S1 to S4, the tepals finally turned dark red when the flowers opened.

Anthocyanin biosynthesis has always been a research hotspot of plant secondary metabolism research, and the corresponding genes include *PAL*, *C4H*, *4CL*, *CHS*, *CHI*, *F3H*, *F3'H*, *DFR*, *ANS*, and *UFGT* [1, 49]. Anthocyanin pathway genes play important roles in flower coloration [50, 51]. Chalcone synthase encoded by the *CHS* gene is a core enzyme involved in anthocyanin biosynthesis, and decreasing the expression of *CHS* can lead to the fading of flower color [52]. Using RNA interference technology to reduce the transcript level of *F3H* gene in summer viola, the flower color changed from blue-purple to white [53]. Similar results have been reported for calli [54], morning glories [55], and *Phalaenopsis amabilis* [56]. In 'Royal Velvet,' most of the anthocyanin biosynthesis enzyme genes identified from transcriptome data were at a low expression level in S1 and markedly upregulated at S2 and S3 (Fig. 4), displaying a strong correlation between their mRNA levels and anthocyanin concentration in the tepals. The anthocyanin content reached its peak and resulted in a dark red color in S4, when the expression levels of seven *CHS* (DN10975_c0_g1, DN10975_c0_g2, DN18610_c0_g1, DN26330_c0_g1, DN3694_c0_g1, DN4815_c0_g1, DN9689_c0_ g1), one *CHI* (DN2556_c1_g1), one *F3'H* (DN9264_c0_g1), one

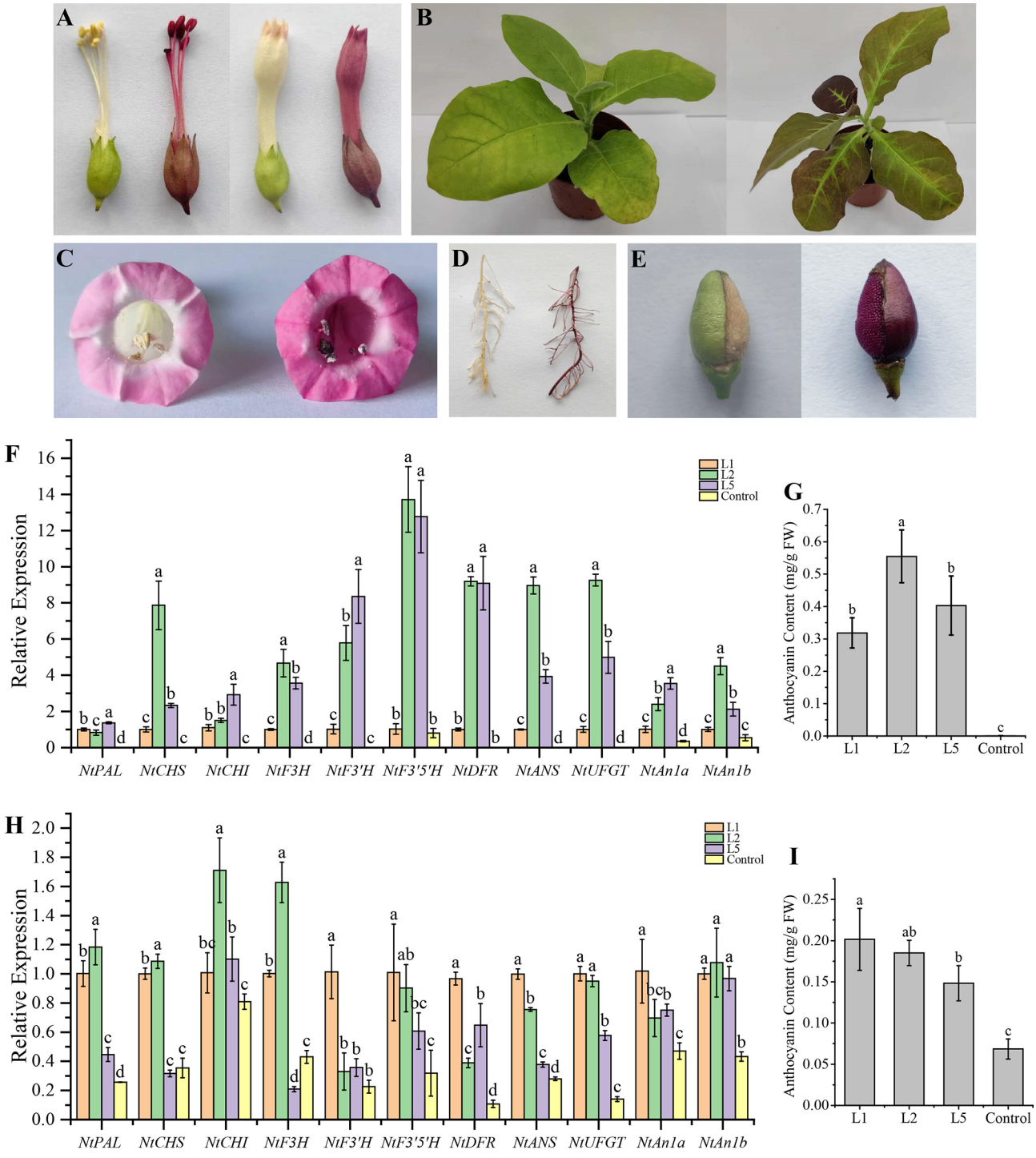

Fig. 8 Overexpression of*HpMYB1*strongly promoted anthocyanin accumulation in tobacco. (**A**) Flower, filaments, anthers, stigma and sepal phenotypes of overexpressing (OE)-*HpMYB1* line (left) and control (right). (**B**) Leaf phenotypes of OE-*HpMYB1* line and control. (C) Corolla phenotypes of OE-*HpMYB1* line and control. (**D**) Root phenotypes of OE-*HpMYB1* line and control. (**E**) Ovary wall and seed coat phenotypes of OE-*HpMYB1* line and control. (**F**) and (**G**) represent the relative expression profles of anthocyanin-related genes and anthocyanin content of the OE-*HpMYB1* lines, respectively. (**H**) and (**I**) represent the relative expression profles of anthocyanin-related genes and anthocyanin content of the control plant respectively. L1, L2, and L5 mean three transgenic tobacco lines of OE-*HpMYB1* and the *NtActin* were used as the reference gene

DFR (DN8170_c0_g1), one *ANS* (DN5468_c0_g1), and one *UFGT* (DN19097_c0_g1) were high, suggesting their important roles in the coloration of mature tepals.

HpMYB1 is a functional R2R3-MYB TF involved in regulating anthocyanin biosynthesis

It has been revealed that the binding of R2R3-MYB TFs to the promoter of anthocyanin structural genes strongly induces their expression and anthocyanin accumulation [18, 57, 58]. In apples, *MdMYB1* can act as an activator to regulate the expression of anthocyanin pathway genes and determine skin color [59]. Overexpression of an anthocyanin-promoting R2R3-MYB TF, GMYB10, significantly increased the anthocyanin content and induced the production of new anthocyanins in *Gerbera hybrida* [22, 60]. In the present study, we found that HpMYB1 contains a conserved bHLH motif in the R3 domain (Fig. 7B), suggesting that the combination of HpMYB1 with bHLH TFs co-regulates anthocyanin biosynthesis, which has been reported in many other plant species [13, 61]. Our phylogenetic analysis showed that HpMYB1 is an anthocyanin-specific MYB activator in the AN2 subgroup and is closely related to MaMybA (Fig. 7A), a known anthocyanin-related R2R3-MYB TF isolated from *Muscari armeniacum* flowers [62]. The gene expression profiles of *HpMYB1* were in accordance with those of most anthocyanin biosynthetic genes in 'Royal Velvet,' such as *HpC4H*, *Hp4CL*, *HpCHS2*, *HpCHI*, *HpF3H*, *HpF3'H1*, *HpDF*R, and *HpUFGT* (Fig. 5). More importantly, heterologous expression of *HpMYB1* in tobacco resulted in higher anthocyanin concentrations in both vegetative and reproductive tissues, and strong activation of anthocyanin-related genes was observed in the transgenic lines compared to those in the control plants (Fig. 8). Therefore, we hypothesized that *HpMYB1* is a R2R3-MYB transcriptional activator involved in regulating anthocyanin biosynthesis in 'Royal Velvet' tepals. Functional verification of *HpMYB1* in *H.* × *hybridum* calli was also performed (data not shown).

Conclusions

In this study, a de novo assembly of transcriptome data was performed to provide preliminary insights into the mechanisms of anthocyanin accumulation in the four stages of 'Royal Velvet' tepal development. The unigene expression pattern analysis revealed that anthocyanin biosynthesis-related genes were significantly upregulated in S2 and S3. An R2R3-MYB TF, *HpMYB1*, involved in anthocyanin biosynthesis regulation, was identified by RNA-seq analysis, and its mRNA profiles were in accordance with those of most anthocyanin structural genes and verified by qRT-PCR analysis. Furthermore, the stable genetic transformation of *HpMYB1* strongly increased the pigment levels in various tissues and activated anthocyanin-related genes in tobacco. Our results lay the foundation for understanding the molecular mechanisms underlying the accumulation of anthocyanins and flower coloration in *H.*× *hybridum.*

Materials and methods

Plants and materials

Bulbs of *H.* × *hybridum* 'Royal Velvet' with a circumference of 30–32 cm were purchased from Guangdong Shengyin Flower and Gardening Co., LTD. They were stored at 4±1℃ for about 45 days to break dormancy. Subsequently, they were planted in the greenhouse of the South China Botanical Garden, Chinese Academy of Sciences (Guangzhou, China). The flower development of 'Royal Velvet' can be divided into four stages: Stage 1 (S1): Flower buds are encased in bracts, almost no pigment is present (lasting for three days); Stage 2 (S2): The flower buds are just emerging from the bract, pigment begins to accumulate (lasting for six days); Stage 3 (S3): Flowers are about to bloom with obvious pigment accumulation (lasting for nine days); Stage 4 (S4): Flowers in full bloom with dark-red pigment coloration (lasting for 12 days). The phenotypes of the four flower developmental stages are shown in Supplementary Fig. S1. Tepal tissue samples were collected between 10 a.m. and 11 a.m. on May 2020. Tobacco (*Nicotiana tabacum* 'NC89') used for subsequent experiments was cultivated in a long-day phytotron (16 h/8 h light/dark, 25 °C/18°C). The samples were immediately frozen in liquid nitrogen and stored at -80 °C until further analyses.

Anthocyanin content determination

The tissues of 'Royal Velvet' and tobacco were ground into powder by ball milling, and total anthocyanins were extracted using the pH difference method [63]. Briefly, the powder (0.1 g) was mixed with 2 mL of methanol (containing 0.05% HCl) overnight, after which KCl (0.025 M, pH 1.0) and NaAc (0.4 M, pH 4.5) solutions were used to determine the anthocyanin content. Both solutions (40 μL of each) were mixed with 160 μL aliquot for 15 min in darkness before the measurements. The absorbance at 510 and 700 nm was measured using an ELISA reader (BioTek, Winooski, USA).

RNA preparation and transcriptome sequencing

Total RNA was extracted from 'Royal Velvet' and tobacco tissues using the RNAprep Pure Plant Kit (TIANGEN, China), according to the manufacturer's instructions. Integrity and purity of the total RNA were assessed using a 1% agarose gel and 2100 Bioanalyzer (Agilent Technologies, Palo Alto, CA, USA) and quantified using a NanoDrop 2000 spectrophotometer (Thermo Fisher Scientific, Wilmington DE, USA). Only high-quality RNA samples

were used to construct the sequencing library and analyze the gene expression patterns.

A total of 12 RNA samples of 'Royal Velvet' tepals were used to construct the sequencing libraries using the Illumina TruSeqTM RNA sample preparation kit (San Diego, CA) and sequenced on an Illumina NovaSeq 6,000 platform generating paired-end reads. The clean sequence reads were assembled *de novo* using Trinity (http://trinitytyrnaseq.sourceforge.net/) after filtering the low-quality reads and adaptors. Trinity grouped the transcripts into clusters according to their shared sequence content, and the longest transcript was selected as the unigene. BUSCO software (Version 3.0.2) was used to evaluate the quality of transcriptome assembly. For functional annotation, the assembled unigenes were aligned to public protein databases, including the GO, KEGG, NR, eggNOG, Pfam, and Swiss-Prot databases, using BLASTx. The transcript per million reads (TPM) value was quantified by RSEM software (Version: 1.3.1, http://deweylab.biostat.wisc.edu/rsem/) to calculate the gene expression of each unigene. Differentially expressed genes (DEGs) were identified using the R package DESeq2 for subsequent analysis, and the unigenes with FDR < 0.05 and |Log2 fold change|≥ 1 were considered DEGs. Tools and softwares used in the study were provided in Supplementary Table. S7.

Gene cloning and sequence analysis

Total RNA from the tepals of 'Royal Velvet' at S3 was used to synthesize first strand cDNA using the TransScript® One-Step gDNA Removal cDNA Synthesis SuperMix (Transgen, Beijing, China). Sequences from the transcriptome data were used to design specific primers using the SnapGene software (V2.3.2). Full-length cDNA of *HpMYB1* was amplified using the Phanta Max Super-Fidelity DNA Polymerase (Vazyme Biotech Co., Ltd., Nanjing, China). The PCR products were cloned into the pEASY®-Blunt Cloning Kit (TransGen Biotech Co., Ltd.; Beijing, China) and sequenced. For the phylogenetic analysis and sequence alignment, full-length deduced amino acid sequences were analyzed using the DNAMAN (v 8.0.8.789) and MEGA (v 7.0.26) programs (neighbor-joining method with 1000 bootstrap replicates), respectively.

Subcellular localization

A fragment of *HpMYB1* containing ORF was inserted into the *Eco*RI and *Bam*HI sites of the pSAT6-EYFP-N1 vector to create the recombinant plasmid 35 S::HpMYB1-YFP, which was driven by the CaMV 35 S promoter. The control vector 35 S::YFP, nuclear marker 35 S::mcherry, and 35 S::HpMYB1-YFP were introduced by polyethylene glycol (PEG)-mediated transient transformation [64]. After culture at 28 °C in darkness for 16 h, the protoplasts were examined under a Zeiss LSM 510 confocal microscope (Zeiss, Jena, Germany) with a cooled digital CCD camera (Zeiss, Jena, Germany) for imaging.

qRT-PCR analysis

qRT-PCR was performed to investigate the gene expression levels in 'Royal Velvet' and tobacco tissues and validate the expression profile data of RNA-seq. Total RNA extraction and first-strand cDNA synthesis were performed using the kits described above. Polymerase chain reactions were conducted in a LightCycler 480 II system (Roche, Mannheim, Germany) using the PerfectStart Green qPCR SuperMix (TransGen Biotech Co., Ltd., Beijing, China). The total reaction volume was 20 μL, containing 1 μL of the cDNA template. The amplification was programmed as follows: 94℃ for 30 s, 45 cycles at 94℃ for 5 s, 60℃ for 30 s. The cycle threshold (Ct) values were calculated using the LightCycler 480 software (v1.5.1.62) and the relative gene expression was estimated with the $2^{-\Delta\Delta CT}$ method [65]. *HpEF-1a*, *HpGAPDH2* [66] and *NtActin* (accession number: X69885) were used as reference genes.

Overexpression of *HpMYB1* in Tobacco

To determine the function of HpMYB1, the ORF of *HpMYB1* without stop codons was inserted into the *Eco*R I and *Xba* I sites of the pGreen-C17 vector driven by the CaMV 35 S promoter. The recombinant plasmid pGreen-C17-HpMYB1 was transferred into *Agrobacterium tumefaciens* strain EHA105 using the freeze-thaw method and then transformed into tobacco using the leaf disc method [67]. T1-generation corollas and leaves from transgenic and control tobacco plants were collected for anthocyanin content determination and qRT-PCR analysis.

Statistical analysis

All charts were plotted with average values and standard errors of the parameters using Origin Pro (2021) (v9.8.0.200). Statistical significance was tested by one-way ANOVA followed by Duncan's (D) test using the SPSS software (v 25.0), with a significance level of $p < 0.05$. All measurements were performed in triplicates.

Abbreviations

DEGs	Differentially expressed genes
TF	Transcription factor
NR	Non-redundant protein sequence database
KEGG	Kyoto Encyclopedia of Genes and Genomes
GO	Gene Ontology
eggNOG	evolutionary genealogy of genes:Non-supervised Orthologous Groups
Pfam	Protein family
Swiss-Prot	Swiss-Prot Protein Sequence Database
qRT-PCR	Quantitative real-time polymerase chain reaction
RACE	Rapid-amplification of cDNA ends
Ct	cycle threshold
TPM	Transcript per million reads
CaMV	cauliflower mosaic virus

ORF	Open reading frame
RNA-seq	RNA sequencing

Supplementary Information

The online version contains supplementary material available at https://doi.org/10.1186/s12870-023-04582-4.

Supplementary Material 1

Supplementary Material 2

Acknowledgements
The authors thank Jingjue Zeng for her assistance in collecting and cultivating the plant materials of *Hippeastrum hybridum*. We acknowledge the Shanghai Majorbio Bio-pharm Biotechnology for technical assistance in RNA-seq data analysis.

Authors' contributions
J.L., L.F., and S.Z. initiated the project and designed experiments; J.L. performed the experiments; J.L., L.F., and S.Z. analyzed the data and wrote the manuscript; K.W., G.M., and L.L. provided useful advice.

Funding
This work was funded by the Guangdong Key Technology Research and Development Program (2020B020220005), the Science and Technology Projects in Guangdong (2023A1515010237), the Key-Field Research and Development Program of Guangdong Province (2022B1111230001), the 2021 Dongguan Provincial Rural Revitalization Program (20211800400022), the Guangdong Modern Agricultural Industry Technology System Program (2023KJ121).

Availability of data and material
The raw data of the 12 samples used in the present study were submitted to the NCBI Short Read Archive (SRA) under the BioProject accession number PRJNA943557.

Declarations

Competing interests
The authors declare no competing interests.

Ethics approval and consent to participate
The collection of plant materials used in this study complied with institutional and national guidelines. The field studies were conducted in accordance with local legislation.

Consent for publication
Not applicable.

Received: 6 April 2023 / Accepted: 3 November 2023
Published online: 28 November 2023

References

1. Tanaka Y, Sasaki N, Ohmiya A. Biosynthesis of plant pigments: anthocyanins, betalains and carotenoids. Plant J. 2008;54(4):733–49.
2. Winkel-Shirley B. Flavonoid biosynthesis. A colorful model for genetics, biochemistry, cell biology, and biotechnology. Plant Physiol. 2001;126(2):485–93.
3. Diaconeasa Z, Stirbu I, Xiao JB, Leopold N, Ayvaz Z, Danciu C, Ayvaz H, Stanila A, Nistor M, Socaciu C. Anthocyanins, vibrant color pigments, and their role in Skin cancer prevention. Biomedicines. 2020;8(9):336.
4. Martin C, Prescott A, Mackay S, Bartlett J, Vrijlandt E. Control of anthocyanin biosynthesis in flowers of *Antirrhinum majus*. Plant J. 1991;1(1):37–49.
5. Schaefer HM, Schaefer V, Levey DJ. How plant-animal interactions signal new insights in communication. Trends Ecol Evol. 2004;19(11):577–84.
6. Petroni K, Pilu R, Tonelli C. Anthocyanins in corn: a wealth of genes for human health. Planta. 2014;240(5):901–11.
7. Tsuda T. Dietary anthocyanin-rich plants: biochemical basis and recent progress in health benefits studies. Mol Nutr Food Res. 2012;56(1):159–70.
8. Saito K, Yonekura-Sakakibara K, Nakabayashi R, Higashi Y, Yamazaki M, Tohge T, Fernie AR. The flavonoid biosynthetic pathway in *Arabidopsis*: structural and genetic diversity. Plant Physiol Bioch. 2013;72:21–34.
9. Holton TA, Cornish EC. Genetics and biochemistry of anthocyanin biosynthesis. Plant Cell. 1995;7(7):1071–83.
10. Quattrocchio F, Wing JF, Leppen HTC, Mol JNM, Koes RE. Regulatory genes-controlling anthocyanin pigmentation are functionally conserved among plant-species and have distinct sets of target genes. Plant Cell. 1993;5(11):1497–512.
11. Zhao J, Dixon RA. The 'ins' and 'outs' of flavonoid transport. Trends Plant Sci. 2010;15(2):72–80.
12. Hichri I, Barrieu F, Bogs J, Kappel C, Delrot S, Lauvergeat V. Recent advances in the transcriptional regulation of the flavonoid biosynthetic pathway. J Exp Bot. 2011;62(8):2465–83.
13. Xu WJ, Dubos C, Lepiniec L. Transcriptional control of flavonoid biosynthesis by MYB-bHLH-WDR complexes. Trends Plant Sci. 2015;20(3):176–85.
14. Cone KC, Burr FA, Burr B. Molecular analysis of the maize anthocyanin regulatory locus *C1*. P Natl Acad Sci USA. 1986;83(24):9631–5.
15. Paz-Ares J, Ghosal D, Wienand U, Peterson PA, Saedler H. The regulatory *C1* locus of Zea mays encodes a protein with homology to myb proto-oncogene products and with structural similarities to transcriptional activators. EMBO J. 1987;6(12):3553–8.
16. Tohge T, Nishiyama Y, Hirai MY, Yano M, Nakajima J, Awazuhara M, Inoue E, Takahashi H, Goodenowe DB, Kitayama M, et al. Functional genomics by integrated analysis of metabolome and transcriptome of Arabidopsis plants over-expressing an MYB transcription factor. Plant J. 2005;42(2):218–35.
17. Gonzalez A, Zhao M, Leavitt JM, Lloyd AM. Regulation of the anthocyanin biosynthetic pathway by the TTG1/bHLH/Myb transcriptional complex in *Arabidopsis* seedlings. Plant J. 2008;53(5):814–27.
18. Pattanaik S, Kong Q, Zaitlin D, Werkman JR, Xie CH, Patra B, Yuan L. Isolation and functional characterization of a floral tissue-specific R2R3 MYB regulator from Tobacco. Planta. 2010;231(5):1061–76.
19. Yamagishi M, Shimoyamada Y, Nakatsuka T, Masuda K. Two *R2R3-MYB* genes, homologs of Petunia *AN2*, regulate anthocyanin biosyntheses in flower tepals, tepal spots and leaves of asiatic hybrid lily. Plant Cell Physiol. 2010;51(3):463–74.
20. Li CH, Qiu J, Yang GS, Huang SR, Yin JM. Isolation and characterization of a R2R3-MYB transcription factor gene related to anthocyanin biosynthesis in the spathes of *Anthurium andraeanum* (Hort). Plant Cell Rep. 2016;35(10):2151–65.
21. Hsu CC, Chen YY, Tsai WC, Chen WH, Chen HH. Three R2R3-MYB transcription factors regulate distinct floral pigmentation patterning in *Phalaenopsis* spp. Plant Physiol. 2015;168(1):175–U910.
22. Elomaa P, Uimari A, Mehto M, Albert VA, Laitinen RAE, Teeri TH. Activation of anthocyanin biosynthesis in *Gerbera hybrida* (Asteraceae) suggests conserved protein-protein and protein-promoter interactions between the anciently diverged monocots and eudicots. Plant Physiol. 2003;133(4):1831–42.
23. Li J, Wu KL, Li L, Ma GH, Fang L, Zeng SJ. AcMYB1 interacts with AcbHLH1 to regulate anthocyanin biosynthesis in *Aglaonema commutatum*. Front Plant Sci 2022, 13.
24. Zhang YZ, Xu SZ, Ma HP, Duan XJ, Gao SX, Zhou XJ, Cheng YW. The R2R3-MYB gene *PsMYB58* positively regulates anthocyanin biosynthesis in tree peony flowers. Plant Physiol Bioch. 2021;164:279–88.
25. Luan YT, Tang YH, Wang X, Xu C, Tao J, Zhao DQ. Tree peony R2R3-MYB transcription factor *PsMYB30* promotes petal blotch formation by activating the transcription of anthocyanin synthase gene. Plant Cell Physiol. 2022;63(8):1101–16.
26. Li YQ, Shan XT, Tong LN, Wei C, Lu KY, Li SY, Kimani S, Wang SC, Wang L, Gao X. The conserved and particular roles of the R2R3-MYB regulator FhPAP1 from *Freesia hybrida* in flower anthocyanin biosynthesis. Plant Cell Physiol. 2020;61(7):1365–80.
27. Inkham C, Piriyapongpitak P, Ruamrungsri S. Storage and growth temperatures affect growth, flower quality, and bulb quality of *Hippeastrum*. Hortic Environ Biote. 2019;60(3):357–62.
28. Sutlana J, Sutlana N, Siddique M, Islam A, Hossain MM, Hossain TJJCEA. *In vitro* bulb production in *Hippeastrum* (*Hippeastrum Hybridum*). J Cent Eur Agric. 2010;11(4):469–74.

29. Silberbush M, Ephrath JE, Alekperov C, Ben-Asher J. Nitrogen and potassium fertilization interactions with carbon dioxide enrichment in *Hippeastrum* bulb growth. Sci Hortic. 2003;98(1):85–90.
30. Zayed R, El-Shamy H, Berkov S, Bastida J, Codina C. In vitro micropropagation and alkaloids of *Hippeastrum vittatum*. In Vitro Cell Dev Biol Plant. 2011;47:695–701.
31. Marciniak P, Jędrzejuk A, Sochacki D. Evaluation of the possibility of obtaining viable seeds from the cross-breeding *Hippeastrum* × *chmielii* chm. With selected cultivars of *Hippeastrum Hybridum* Hort. Folia Hortic. 2021;33(1):185–94.
32. Cho N, Du YL, Valenciano AL, Fernandez-Murga ML, Goetz M, Clement J, Cassera MB, Kingston DGI. Antiplasmodial alkaloids from bulbs of *Amaryllis belladonna* Steud. Bioorg Med Chem Lett. 2018;28(1):40–2.
33. Wang Y, Chen DF, He XF, Shen JX, Xiong M, Wang X, Zhou D, Wei ZZ. Revealing the complex genetic structure of cultivated amaryllis (*Hippeastrum Hybridum*) using transcriptome-derived microsatellite markers. Sci Rep 2018, 8.
34. Byamukama R, Jordheim M, Kiremire B, Namukobe J, Andersen ØM. Anthocyanins from flowers of *Hippeastrum* cultivars. Sci Hortic. 2006;109(3):262–6.
35. Li J, Wu K, Li L, Ma G, Fang L, Zeng S. Transcriptomic analysis reveals biosynthesis genes and transcription factors related to leaf anthocyanin biosynthesis in *Aglaonema commutatum*. BMC Genom. 2023;24(1):28.
36. Bao XM, Zong Y, Hu N, Li SM, Liu BL, Wang HL. Functional R2R3-MYB transcription factor *NsMYB1*, regulating anthocyanin biosynthesis, was relative to the fruit color differentiation in *Nitraria Sibirica* Pall. BMC Plant Biol 2022, 22(1).
37. Lou Q, Liu YL, Qi YY, Jiao SZ, Tian FF, Jiang L, Wang YJ. Transcriptome sequencing and metabolite analysis reveals the role of delphinidin metabolism in flower colour in grape hyacinth. J Exp Bot. 2014;65(12):3157–64.
38. Cui XQ, Deng JL, Huang CY, Tang X, Li XM, Li XL, Lu JS, Zhang ZB. Transcriptomic analysis of the anthocyanin biosynthetic pathway reveals the molecular mechanism associated with purple color formation in *Dendrobium* Nestor. Life-Basel 2021, 11(2).
39. Li X, Wang Z, Yang LY, Xu JX, Zhang YC. Expression level of B- and C-class MADS-box genes is associated with the petaloidy of stamens in cultivated amaryllis (*Hippeastrum Hybridum*). J Hortic Sci Biotech. 2022;97(2):211–23.
40. Wang QM, Cui JG, Dai HY, Zhou YB, Li N, Zhang ZH. Comparative transcriptome profiling of genes and pathways involved in leaf-patterning of Clivia miniata var. Variegata. Gene. 2018;677:280–8.
41. Li X, Tang DQ, Du H, Shi YM. Transcriptome sequencing and biochemical analysis of perianths and coronas reveal flower color formation in *Narcissus pseudonarcissus*. Int J Mol Sci 2018, 19(12).
42. Tanaka Y, Ohmiya A. Seeing is believing: engineering anthocyanin and carotenoid biosynthetic pathways. Curr Opin Biotech. 2008;19(2):190–7.
43. Iwashina T. Contribution to flower colors of flavonoids including anthocyanins: a review. Nat Prod Commun. 2015;10(3):529–44.
44. Peng JQ, Dong XJ, Xue C, Liu ZM, Cao FX. Exploring the molecular mechanism of blue flower color formation in *Hydrangea macrophylla* cv. Forever summer. Front Plant Sci 2021, 12.
45. Fang ZW, Hou ZH, Wang SP, Liu ZX, Wei SD, Zhang YX, Song JH, Yin JL. Transcriptome analysis reveals the accumulation mechanism of anthocyanins in buckwheat (*Fagopyrum esculentum* Moench) cotyledons and flowers. Int J Mol Sci 2019, 20(6).
46. Mizuta D, Ban T, Miyajima I, Nakatsuka A, Kobayashi N. Comparison of flower color with anthocyanin composition patterns in evergreen azalea. Sci Hortic. 2009;122(4):594–602.
47. Rothenberg DO, Yang HJ, Chen MB, Zhang WT, Zhang LY. Metabolome and transcriptome sequencing analysis reveals anthocyanin metabolism in pink flowers of anthocyanin-rich tea (*Camellia sinensis*). Molecules 2019, 24(6).
48. Guo LP, da Silva JAT, Pan QH, Liao T, Yu XN. Transcriptome analysis reveals candidate genes involved in anthocyanin biosynthesis in flowers of the pagoda tree (*Sophora japonica* L). J Plant Growth Regul. 2022;41(1):1–14.
49. Cheynier V, Comte G, Davies KM, Lattanzio V, Martens S. Plant phenolics: recent advances on their biosynthesis, genetics, and ecophysiology. Plant Physiol Bioch. 2013;72:1–20.
50. Han YP, Vimolmangkang S, Soria-Guerra RE, Rosales-Mendoza S, Zheng DM, Lygin AV, Korban SS. Ectopic expression of apple *F3'H* genes contributes to anthocyanin accumulation in the Arabidopsis *tt7* mutant grown under nitrogen stress. Plant Physiol. 2010;153(2):806–20.
51. Koes R, Verweij W, Quattrocchio F. Flavonoids: a colorful model for the regulation and evolution of biochemical pathways. Trends Plant Sci. 2005;10(5):236–42.
52. Vanderkrol AR, Mur LA, Delange P, Mol JNM, Stuitje AR. Inhibition of flower pigmentation by antisense CHS genes: promoter and minimal sequence requirements for the antisense effect. Plant Mol Biol. 1990;14(4):457–66.
53. Ono E, Fukuchi-Mizutani M, Nakamura N, Fukui Y, Yonekura-Sakakibara K, Yamaguchi M, Nakayama T, Tanaka T, Kusumi T, Tanaka Y. Yellow flowers generated by expression of the aurone biosynthetic pathway. P Natl Acad Sci USA. 2006;103(29):11075–80.
54. Seitz C, Oswald N, Borstling D, Forkmann G, Martens S. Being acyanic: an unavoidable fate for many white flowers? Acta Hortic 2003(612):83–8.
55. Morita Y, Ishiguro K, Tanaka Y, Iida S, Hoshino A. Spontaneous mutations of the UDP-glucose:flavonoid 3-O-glucosyltransferase gene confers pale- and dull-colored flowers in the Japanese and common morning glories. Planta. 2015;242(3):575–87.
56. Meng XQ, Li G, Gu LY, Sun Y, Li ZY, Liu JR, Wu XQ, Dong TT, Zhu MK. Comparative metabolomic and transcriptome analysis reveal distinct flavonoid biosynthesis regulation between petals of white and purple *Phalaenopsis Amabilis*. J Plant Growth Regul. 2020;39(2):823–40.
57. Shen GA, Wu RR, Xia YY, Pang YZ. Identification of transcription factor genes and functional characterization of *PlMYB1* from *Pueraria lobata*. Front Plant Sci 2021, 12.
58. Huang D, Xu SQ, Qin YH, Li YJ, Ming RH, Huang RS, Wang JH, Tan Y. Comparative transcriptomic analysis identifies KcMYB1 as a R2R3-MYB anthocyanin activator in *Kadsura Coccinea*. Plant Sci 2022, 324.
59. Takos AM, Jaffe FW, Jacob SR, Bogs J, Robinson SP, Walker AR. Light-induced expression of a *MYB* gene regulates anthocyanin biosynthesis in red apples. Plant Physiol. 2006;142(3):1216–32.
60. Laitinen RAE, Ainasoja M, Broholm SK, Teeri TH, Elomaa P. Identification of target genes for a MYB-type anthocyanin regulator in *Gerbera hybrida*. J Exp Bot. 2008;59(13):3691–703.
61. Deng CY, Wang JY, Lu CF, Li YF, Kong DY, Hong Y, Huang H, Dai SL. CcMYB6-1 and CcbHLH1, two novel transcription factors synergistically involved in regulating anthocyanin biosynthesis in cornflower. Plant Physiol Bioch. 2020;151:271–83.
62. Chen KL, Du LJ, Liu HL, Liu YL. A novel R2R3-MYB from grape hyacinth, MaMybA, which is different from *MaAN2*, confers intense and magenta anthocyanin pigmentation in Tobacco. Bmc Plant Biol 2019, 19(1).
63. Wrolstad RE, Culbertson JD, Cornwell CJ, Mattick LR. Detection of adulteration in blackberry juice concentrates and wines. J Assoc off Ana Chem. 1982;65(6):1417–23.
64. Yoo SD, Cho YH, Sheen J. *Arabidopsis* mesophyll protoplasts: a versatile cell system for transient gene expression analysis. Nat Protoc. 2007;2(7):1565–72.
65. Livak KJ, Schmittgen TD. Analysis of relative gene expression data using real-time quantitative PCR and the 2(T)(-Delta Delta C) method. Methods. 2001;25(4):402–8.
66. Liu XT, Wang SL, Xue JQ, Xue YQ, Lu YM, Zhang XX. Selection of reference genes for quantitative real-time PCR in different tissue and organ of barbadoslily. Acta Hortic Sini. 2018;45(5):919–30.
67. Zhang MM, Ji LS, Xue H, Yang YT, Wu CA, Zheng CC. High transformation frequency of Tobacco and rice via *Agrobacterium*-mediated gene transfer by flanking a Tobacco matrix attachment region. Physiol Plant. 2007;129(3):644–51.

Publisher's Note